Large scale integration of CVD-graphene based NEMS with narrow distribution of resonance parameters

Hadi Arjmandi-Tash,[1, a)] Adrien Allain,[1, b)] Zheng (Vitto) Han,[1, c)] and Vincent Bouchiat[1]

University of Grenoble Alpes, CNRS, Institut Néel, F-38000 Grenoble, France.

We present a novel method for the fabrication of the arrays of suspended micron-sized membranes, based on monolayer pulsed-CVD graphene. Such devices are the source of an efficient integration of graphene nano-electro-mechanical resonators, compatible with production at the wafer scale using standard photolithography and processing tools. As the graphene surface is continuously protected by the same polymer layer during the whole process, suspended graphene membranes are clean and free of imperfections such as deposits, wrinkles and tears. Batch fabrication of 100 micrometers-long multi-connected suspended ribbons is presented. At room temperature, mechanical resonance of electrostatically-actuated devices show narrow distribution of their characteristic parameters with high quality factor and low effective mass and resonance frequencies, as expected for low stress and adsorbate-free membranes. We show that such devices possesses outstanding force and mass sensing characteristics. Upon cooling, a sharp increase of both resonant frequency and quality factor is observed, enabling to extract the thermal expansion coefficient of CVD graphene. Comparison with state-of-the-art graphene NEMS is presented.

[a)]h.arjmandi.tash@lic.leidenuniv.nl; Present address: Leiden Institute of Chemistry, Faculty of Science, Leiden University, Leiden, The Netherlands.

[b)]Present address: Laboratory of Nanoscale Electronics and Structures, École Polytechnique Fédérale de Lausanne, Station 17, CH-1015, Lausanne, Switzerland.

[c)]Present address: Institute of Metal Research Chinese Academy of Sciences, Shenyang, Liaoning, 110016, China.

I. INTRODUCTION

Graphene appeared [1] as an unique active material for the realization of ultimately-thin mechanically vibrating membranes. It combines in a same material some unique features: being ultimately thin and made of carbon, a light element, graphene possesses also extremely high Young's modulus [2] thanks to the carbon-carbon sigma bonds. Furthermore, semi-metallic properties of graphene makes electrical actuation possible while its high electronic mobility enables self-detection [3] of the mechanical resonance; further extending to 2D membranes the pioneer field of sp^2 carbon-based nanoelectromechanical systems (NEMS) which started with carbon nanotubes [4]. By far, most of the studies[1,3,5–7] have been performed using flakes of exfoliated graphene, where the NEMS device is fabricated using either electrodes alignment [1,3,5,7] or micromanipulation and stamping [6,8].

Graphene produced by chemical vapor deposition (CVD) on copper foils [9] rapidly appeared as an unique technique to produce large sheets of monolayer graphene that can be further transferred onto any arbitrary substrate. It offers a promising route for the scalable fabrication of graphene NEMS [10,11], suitable for radio frequencies [8] or optomechanical [12] applications. However, defects occurring either during CVD synthesis (such as grain boundaries and multilayers patches) or during the further transfer and fabrication of graphene on the host substrate (such as polymer residues, ripples, stress induced by photoresist) generates inhomogeneities in the graphene membrane, leading to a significant dispersion of the NEMS resonance parameters.

The idea which is followed in this work is to protect the graphene surface during the fabrication process to prevent exposure to contaminations. Graphene surface protection is already known as an essential precaution for preserving the high quality of CVD graphene during electronic device fabrication [13]. In the process presented in this work, the polymer (spin-coated PMMA layer) that is usually used to handle the graphene sheet during wet transfer, is further used for two additional purposes: (i) as a *photo lithography resist* during the ribbon formation by plasma etching, and, (ii) as a *protection blanket* to further protect graphene during the entire fabrication.

The comparison of the room temperature resonance characteristics of our devices with reported similar samples (both exfoliated and CVD graphene) confirms the competence of our samples for sensing applications. Indeed narrow distribution of the resonance parameters

promises reproducibility of the results. Additionally, we show that the improved fabrication method leads to boosting the quality factor of the resonators, reaching fundamental limits. The achieved ultra-clean and defect-free membranes suit best for fundamental researches: the modulation of the resonance frequency due to the thermal stress at low temperature allows us to experimentally extract the coefficient of the thermal expansion of CVD graphene for the first time.

II. LARGE SCALE INTEGRATION OF ARRAYS OF SUSPENDED GRAPHENE MEMBRANES

The graphene is first synthesized by chemical vapor deposition on copper following the classical method [9] but using a variation involving pulsed-injection of methane, which is known[14] to inhibit multilayer patches at the macroscale. Such a growth process leads to homogeneous, strictly monolayered graphene with typical single crystal grain size exceeding 30 micrometers. The graphene layer is then covered with a PMMA resist layer and the copper substrate is etched using ammonium persulfate solution (see methods). In the following steps, we are modifying the NEMS fabrication technique previously adapted to batch processing of CVD-based graphene NEMS[11].

This involves keeping the graphene ribbon covered with PMMA supporting polymer during the full process. This is done by using two different types of polymer resists (respectively PMMA and commercial photoresist) which are selectively removed by different solvents (respectively MIBK and water-based developer), enabling to keep the initial PMMA support layer intact during the two lithography steps required for graphene ribbon patterning and electrode deposition. Finally, the fabrication process terminates by under-etching the ribbon using buffered HF solution followed by drying using a CO_2 critical point dryer. The full details of the process flow are presented in the method section. Micrographs of final stage of a typical set of devices is shown in Figure 1. The devices present a series of independently labeled chip with set of electrodes connecting graphene ribbons presenting variable width and length. Each chip involves a pattern of 36 connecting gold electrodes, surrounding a 130-microns-long suspended graphene ribbon. This ribbon defines a linear array of graphene membranes nano-mechanical resonators. Each chip defines 18 independent devices which can

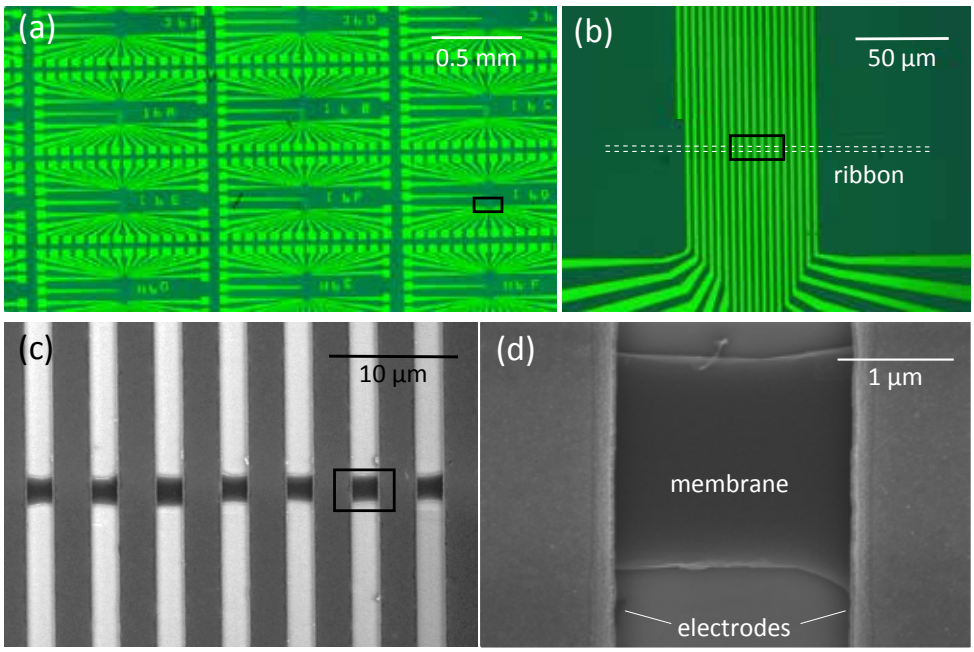

FIG. 1: Large scale integration of NEMS based on doubly clamped graphene membrane a) Optical micrograph showing a fully processed sample. b) Optical micrograph zoomed inside the black rectangle frame depicted in a: The position of the ribbon is illustrated by the dashed lines. c) Scanning electron microscopy (SEM) image zoomed inside the black rectangle frame depicted in b: The figure shows the suspended ribbon connected to the support electrodes. d) SEM image of a single NEMS device membrane showing the absence of deposits and wrinkles.

reach an integration density of 7200 NEMS per cm^2. In the SEM image (Figure 1-d), no contaminant nor wrinkle are seen, indicating the high-quality of the graphene surface. A given ribbon being held by multiple electrodes, each of these acting as a clamp, ripping and slippage of the membrane under the contact is limited under the application of a large mechanical stress and lead to a more homogeneously distributed stress along the ribbon and prevent membrane ripping during cooldown.

III. MEASUREMENTS OF THE VIBRATIONAL PROPERTIES OF GRAPHENE RIBBONS ARRAYS

After the final fabrication step which involves the graphene ribbon protection removal and membrane release, we directly anchor the sample on the cold stage of a cryogenic

probe station equipped with liquid helium flow, allowing continuous electrical measurement in vacuum of the vibrational properties from 300 K down to 10 K. The flexural resonance modes are detected using the frequency modulation detection method[15]. In this scheme, the fundamental flexural mode appears as a peak in the demodulated current circulating through the graphene membrane when one sweeps the excitation frequency across the resonance (see Fig. 2). In the absence of voltage applied on the backgate which induces tension by electrostatic force , resonance frequencies are around 14 MHz, which is comparable to the results obtained on top deposited graphene drums [16] but much lower than the previously reported data for doubly clamped graphene nano-mechanical resonators [7,17,18]. However this value is still above what is predicted by the model (Eq.1 in Supplementary Materials) involving a vibrating membrane in the absence of stress, indicating that built-in stress is present. Indeed, fits using model developed in Singh et al.[7] estimated built-in tensions in our membranes to be around 2.5 nN in average, a value that is approximately 30 times lower compared to this former report (68.6nN) where NEMS are based on exfoliated graphene. The superimposed continuous white line in Fig. 2a shows the best fitting with the model introduced in[7] (summarized in the Eq. 3 in Supplementary Materials). Typical extracted parameters from four samples are summarized in table 1.

TABLE I: frequency, effective mass and built-in stress extracted for different samples by analyzing the DC voltage dependence of the flexural modes of $f_0(V_g)$ (fits based on the Eq. 3 in the Supplementary Materials, similar to fig. 2a)

	$f(V_g = 0)[MHz]$	m_{eff}	$\Gamma_0[nN]$
Sample #1	13.15	0.73	2.03
Sample #2	14.12	0.71	2.27
Sample #3	14.06	0.81	2.56
Sample #4	13.62	0.74	2.98

A remarkable feature observed in that extracted parameters resides in the narrow distribution of all fitting parameters, indicating that the ribbons have not only a clean surface but also their built-in stress is low and rather evenly distributed all over the sample, a feature made possible by the large number of electrodes clamping the same ribbon. The comparison of the room temperature resonance properties of our devices with the reported similar

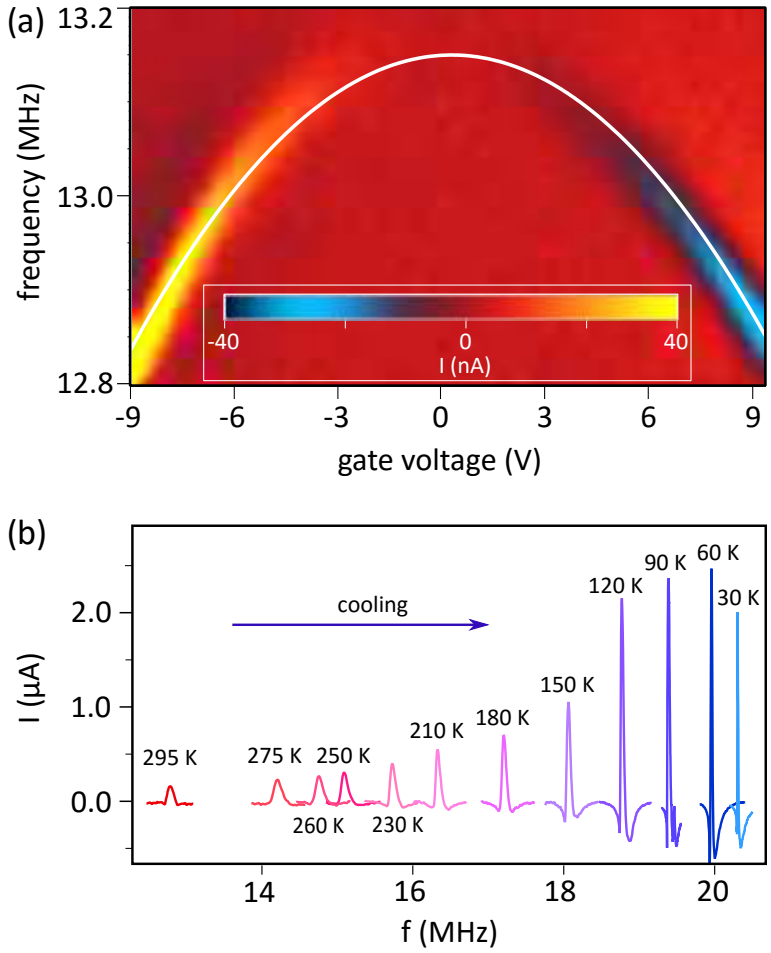

FIG. 2: Frequency dependence of the fundamental flexural mode in graphene ribbons a) dependence of fundamental flexural mode upon application of a DC gate voltage of the mechanical resonance frequency of a typical sample (length and width of $1.26\,\mu m$ and $3.32\,\mu m$): The solid line shows the best fitting using model proposed in Ref.[7] (Eq.3 of Supplementary Materials). b) Resonance spectra of the same mode upon cooling the sample. The measurements were performed while applying a backgate voltage $V_g = -10\,V$.

samples (both exfoliated and CVD graphene) shows a better reproducibility of the device together with a narrow distribution of parameters (table I). Furthermore, for our resonators, the effective mass ranges between 0.71 to 0.81 which is close to the theoretical prediction for the fundamental flexural mode of a doubly-clamped beam of rectangular cross-section, made of pristine, adsorbate-free graphene: $m_{eff}/m = 0.76$ [7,19]. The result further confirms the cleanliness of the membranes. We note that earlier studies of similar NEMS achieved

effective mass m_{eff}/m values ranging between 2.1 [17] to 9.2 [18] and even higher. From that observations, we can conclude that our fabrication process fulfills reproducible production of adsorbate-free graphene NEMS devices.

IV. DISSIPATION MECHANISMS

The quality factor of a resonator is limited by different energy dissipation mechanisms acting in the system; The upper *fundamental* limit, however, is set by the *thermoelastic damping* [20] which is the state of coupling the strain field to a temperature field in a thermoelastic solid. In this condition, the energy of the resonator is dissipated to the environment via an irreversible heat flow driven by the local temperature gradient. The maximum Q factor is given by [20]:

$$Q_{max}^{TE\,-1} = 0.494\,\frac{E\alpha^2 T}{\rho\, C_{p,m}} \tag{1}$$

where T is the temperature, E is the Young's modulus, α is the thermal expansion coefficient, ρ is the density and $C_{p,m}$ is the heat capacity per unit mass at constant pressure of graphene. In supplementary information we show that the thermoelastic damping does not allow the Q of a doubly-clamped resonator to exceed $Q_{max}^{TE} = 308$ at room temperature. We note that Q_{max}^{TE} only depends on the thermoelastic properties of the solids and is unconnected to the geometry.

We use the model presented in Ref [21] (expressed in the Supplementary Information) to calculate the Q in our samples. Supplementary figure 2-b compares our results with former reports. Only the data of the doubly-clamped and monolayer graphene resonators, measured under vacuum and at room temperature are collected here. Interestingly, the resonance quality factor of samples based on exfoliated graphene have been gradually improved during the past years and reached values closed to Q_{max}^{TE} . High populatton of the defect sites occurring during the growth and the absence of an adequate fabrication process, however, have limited the Q in CVD based graphene nanoresonators. To the best of our knowledge, there is only one successful study of CVD graphene based doubly-clamped resonators so far; reporting an average Q of 70. Using the present process, the quality factor averaged on 10 samples is almost three times higher. Our best sample showed $Q = 305$ and reached the limit of thermoelastic damping. We hypothesize that using high-quality starting material

(achieved in pulsed growth CVD) and the improved ribbon-blanketed fabrication method are the major causes for this improvement.

V. TEMPERATURE DEPENDENCE OF THE RESONANCE PROPERTIES

By cooling the sample, thermally induced stress in the membrane affects its resonance frequency. Figure 2-b shows the evolution of the resonance peak of one of our devices (the same sample in Figure 2-a) upon cooling. We have fitted the measured $f_0(T)$ with a third order polynomial function, as shown in Figure 3-a. The extracted quality factors at different temperatures are also depicted in Figure 3-b. Below room temperature ($T < \sim 275\,K$), the quality factor improves while cooling: the temperature dependency of the quality factor is very strong at high temperatures ($\sim 120\,K < T \leq 275\,K$), but becomes weaker when the sample is cold ($T \leq \sim 120\,K$). A dependency of $T^{0.33}$ [22] to $T^{0.36}$ [17,23,24] is proposed for the inverse quality factor of the carbon nanotubes and graphene devices at low temperatures while much stronger dependency of $T^{2.3}$ is observed at high temperatures [22]. We plotted the $T^{0.33}$ and $T^{2.3}$ lines, matching well with our experimental data.

Both the f_0 and Q of the just-cooled sample ($\sim 275\,K < T \leq 295\,K$, as there is a finite distance between the thermometer and the sample, the measured temperature is not necessarily the exact temperature of the sample) exhibit different behavior than the rest of the measured temperature ranges. Cooling the sample increases the f_0; however the increment measured at the first step is more prominent and does not follow the trend of the lower temperatures. The coefficients of the thermal expansion of the material involved (Au [25,26], Si [27] and graphene [28]) do not exhibit any rapid change in this small temperature range which could explain this sharp increment. We attribute the observed behavior to the giant condensation and deposition of the surrounding materials (mainly humidity) on the membrane upon cooling.

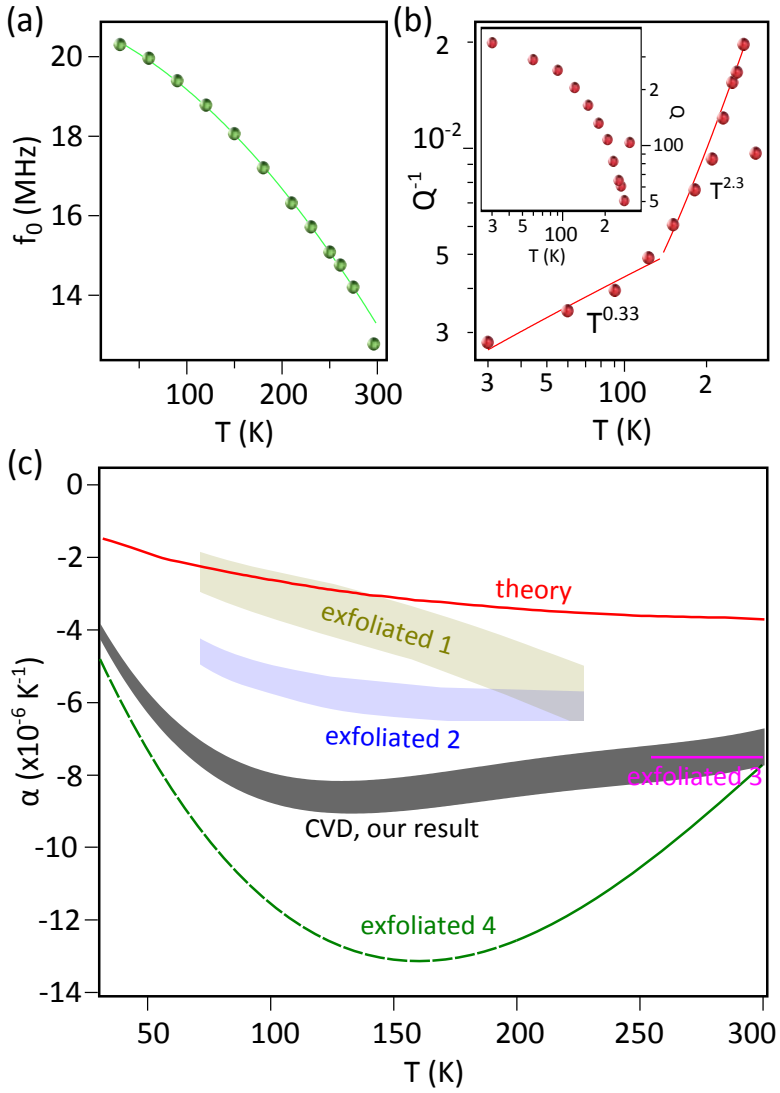

FIG. 3: Low temperature characteristics of our graphene membranes:
a) Extracted resonance frequencies as function of temperature: The solid line shows the best fitting of the data with a polynomial function. b) The inverse quality factor (main panel) and the quality factor (inset) of the same device as a function of the temperature: the solid lines show the $T^{2.3}$ and $T^{0.33}$ dependences. c) Extracted coefficient of thermal expansion (α) of the same device in a and b as a function of the temperature: Result from earlier reports using exfoliated graphene (*exfoliated 1* and *2* from Ref. [7], *exfoliated 3* from Ref. [17], and *exfoliated 4* from Ref. [29]) and a theory prediction [28] are superimposed for comparison. All the data were collected at $Vg = -10\,V$.

VI. DETERMINATION OF THE THERMAL EXPANSION COEFFICIENT OF CVD GRAPHENE

Upon cooling the sample, the thermal stress due to the total expansion/contraction of the materials involved, alters the resonance frequency, as is shown in Figure 3-a. As the linear coefficients of the thermal expansion (CTE, denoted by α) for gold and silicon are well-studied and known, the evolution of the resonance frequency at low temperatures provides information about the CTE of the CVD graphene. We used the already developed model [7] to estimate this parameter (see the Supplementary information for the details of the calculations). The result of the modeling is plotted and compared with earlier reports in Figure 3-c. Especially as a result of the out of plane vibrations of the lattice [28,30], CVD graphene exhibits a negative CTE in the measured temperature range. The CTE of the CVD graphene is in the same range and comparable with the results of the exfoliated graphene [7,17,29]; especially at room temperature, the experimentally measured CTE of all the samples converge to $\alpha \approx -8 \times 10^{-6} K^{-1}$. The similarity of the results with CVD and exfoliated graphene highlights negligible effect of the grain boundaries in the CVD graphene, mainly due to the large grain size achieved in our growth method [31]. CTE of CVD graphene follows the trend predicted theoretical [28] however the values are almost two times larger. Features such as out of plane deformations as a result of static wrinkling of graphene [32] – overlooked in theoretical calculations – should be considered seeking for the origin of the observed deviation. We highlight the fact that the multiconnected feature of our graphene ribbon rules-out the possibility of slippage of the graphene during the experiment which improved the fidelity of our calculations. Indeed the slippage could be a source of uncertainty in the calculation of CTE working with short exfoliated graphene ribbons.

VII. CONCLUSION

We introduced a method for the large-scale production of the high quality free-standing graphene NEMS in which the graphene top surface is continuously covered by the supporting polymer throughout the major steps of the fabrication process. This capping layer not only mechanically supports graphene during ribbon etching but also protects against surface contamination and membrane tearing, leading to defect-free ribbons. The multi-

contacted ribbon design has some advantage regarding stress distribution as each contact acts as a clamp which prevents slippage of the membrane while cooling and allows uniform distribution of the stress; Consequently, narrow distribution of resonance frequencies and moderate increase of frequency due to the addition of stress – compared to the previous reports – achieved. At room temperature, our samples exhibit outstanding quality factors, better than what have been reported earlier for CVD graphene and reaching the fundamental limit. The samples also serve well as mass and force sensors with ultra high sensitivities. We probed the mechanical resonance performance of devices at low temperature. The thermal drift of the resonance frequency allows us to experimentally extract the coefficient of the thermal expansion of CVD graphene in a wide temperature range for the first time. The achieved ultra-clean and defect-free membranes suit best both for fundamental researches and industrial applications.

VIII. MATERIALS AND METHODS

The process flow of the proposed ribbon-blanketed fabrication of CVD graphene based NEMS is illustrated below. Using the process demonstrated in [33] a large CVD graphene sheet supported by a poly(methyl methacrylate)(PMMA) layer is transferred onto a silicon wafer with a $\sim 300\,nm$ thick thermally oxidized surface (a). A long ($\sim 30\,\mathrm{min}$, depending on the exposure dose) illumination with deep ultraviolet (DUV) light through an adequate contact optical mask exposes the PMMA layer to define the ribbon pattern. After the development of the exposed PMMA with MIBK, oxygen plasma etching of unprotected areas achieves long graphene ribbons of typically a 100 microns long and $\sim 2-3\,\mu m$ width (b). Next, metallic electrodes have to be deposited: The whole sample (including the PMMA blanketed graphene ribbons) is spin-coated by LOR3A and UVIII resists (c). Using a suitable mask, short ($\sim 15\,\mathrm{sec}$) DUV illumination exposes the UVIII/LOR3A resists with the final pattern of the electrodes. After the development, the PMMA/graphene ribbons are accessible through the windows opened in the UVIII/LOR3A film (d). Without using any hard mask, a long ($\sim 30\,\mathrm{min}$) DUV illumination exposes the uncovered PMMA areas. After the development and removing the exposed PMMA with MIBK, the graphene ribbons are accessible for metalization (e). Next, Cr (5nm) and Au (70nm) layers are deposited. Lift-off is done by using micro-developer to remove the unnecessary parts of the metals and the UVIII/LOR3A

film. Now, graphene ribbons are electrically connected (f). Up to this point, the surfaces of the membranes have been covered by the same PMMA layer which was initially used for the transferring. This PMMA layer protects the membranes from any mechanical and chemical damages and prevents the deposition of any contaminations on the surface. At this stage, the PMMA layer is stripped away using acetone (g). The fabrication process finishes by under-etching the graphene ribbons using buffered HF solution and drying the suspended membranes in a critical point drying process (h).

IX. ACKNOWLEDGMENTS

The authors are grateful for the help from NanoFab team of Institut Néel. H. Arjmandi Tash acknowledges grant support from the Nanoscience Foundation of Grenoble. This work is partially supported by the French ANR contracts SUPERGRAPH , CLEANGRAPH and DIRACFORMAG, the EU contract NMP3-SL-2010-246073, ERC, EU GRAPHENE Flagship and the Region Rhone-Alpes CIBLE program. The authors are also very thankful to Laëtitia Marty for her valuable comments on analyzing the data and preparing the text.

REFERENCES

[1]J. S. Bunch, A. M. v. d. Zande, S. S. Verbridge, I. W. Frank, D. M. Tanenbaum, J. M. Parpia, H. G. Craighead, and P. L. McEuen, "Electromechanical resonators from graphene sheets," Science **315**, 490 (2007).

[2]C. Lee, X. Wei, J. W. Kysar, and J. Hone, "Measurement of the elastic properties and intrinsic strength of monolayer graphene," Science **321**, 385–388 (2008).

[3]C. Chen, S. Rosenblatt, K. I. Bolotin, W. Kalb, P. Kim, I. Kymissis, H. L. Stormer, T. F. Heinz, and J. Hone, "Performance of monolayer graphene nanomechanical resonators with electrical readout," Nature Nanotechnology **4**, 861–867 (2009).

[4]V. Sazonova, Y. Yaish, H. Ustünel, D. Roundy, T. a. Arias, and P. L. McEuen, "A tunable carbon nanotube electromechanical oscillator." Nature **431**, 284–7 (2004).

[5]A. Eichler, J. Moser, J. Chaste, M. Zdrojek, I. Wilson-Rae, and A. Bachtold, "Nonlinear damping in mechanical resonators made from carbon nanotubes and graphene," Nature Nanotechnology , 1–4 (2011).

[6]V. Singh, S. J. Bosman, B. H. Schneider, Y. M. Blanter, A. Castellanos-Gomez, and G. A. Steele, "Optomechanical coupling between a multilayer graphene mechanical resonator and a superconducting microwave cavity," Nature Nanotechnology , 1–5 (2014).

[7]V. Singh, S. Sengupta, H. S. Solanki, R. Dhall, A. Allain, S. Dhara, P. Pant, and M. M. Deshmukh, "Probing thermal expansion of graphene and modal dispersion at low-temperature using graphene nanoelectromechanical systems resonators." Nanotechnology **21**, 165204 (2010).

[8]X. Song, M. Oksanen, M. A. Sillanpää, H. G. Craighead, J. M. Parpia, and P. J. Hakonen, "Stamp transferred suspended graphene mechanical resonators for radio frequency electrical readout," Nano Letters **12**, 198–202 (2012).

[9]X. Li, W. Cai, J. An, S. Kim, J. Nah, D. Yang, R. Piner, A. Velamakanni, I. Jung, E. Tutuc, S. K. Banerjee, L. Colombo, and R. S. Ruoff, "Large-area synthesis of high-quality and uniform graphene films on copper foils." Science **324**, 1312–1314 (2009), arXiv:0905.1712.

[10]R. A. Barton, B. Ilic, A. M. v. d. Zande, W. S. Whitney, P. L. Mceuen, J. M. Parpia, and H. G. Craighead, "High, size-dependent quality factor in an array of graphene mechanical resonators," Nano Letters **11**, 1232–1236 (2011).

[11]A. M. V. D. Zande, R. A. Barton, J. S. Alden, C. S. Ruiz-Vargas, W. S. Whitney, P. H. Q. Pham, J. Park, J. M. Parpia, H. G. Craighead, and P. L. Mceuen, "Large-scale arrays of single-layer graphene resonators," Nano Letters **10**, 4869–4873 (2010).

[12]R. A. Barton, I. R. Storch, V. P. Adiga, R. Sakakibara, B. R. Cipriany, B. Ilic, S. P. Wang, P. Ong, P. L. Mceuen, J. M. Parpia, and et al., "Photothermal self-oscillation and laser cooling of graphene optomechanical systems," Nano Letters **12**, 4681–4686 (2012).

[13]L. Banszerus, M. Schmitz, S. Engels, M. Goldsche, K. Watanabe, T. Taniguchi, B. Beschoten, and C. Stampfer, "Ballistic transport exceeding 28 μm in cvd grown graphene," Nano Letters **16**, 1387–1391 (2016).

[14]Z. Han, A. Kimouche, D. Kalita, A. Allain, H. Arjmandi-Tash, A. Reserbat-Plantey, L. Marty, S. Pairis, V. Reita, N. BENDIAB, and et al., "Homogeneous optical and electronic properties of graphene due to the suppression of multilayer patches during cvd on copper foils," Advanced Functional Materials **24**, 964–970 (2014).

[15]V. Gouttenoire, T. Barois, S. Perisanu, J.-L. Leclercq, S. T. Purcell, P. Vincent, and A. Ayari, "Digital and fm demodulation of a doubly clamped single-walled carbon-nanotube oscillator: Towards a nanotube cell phone," Small **6**, 1060–1065 (2010).

[16]C. Schwarz, B. Pigeau, L. M. d. Lépinay, A. Kuhn, D. Kalita, N. BENDIAB, L. MARTY, V. Bouchiat, and O. Arcizet, "Deviation from the normal mode expansion in a coupled graphene-nanomechanical system," arXiv preprint arXiv:1601.00154 (2016).

[17]C. Chen, S. Rosenblatt, K. I. Bolotin, W. Kalb, P. Kim, I. Kymissis, H. L. Stormer, T. F. Heinz, and J. Hone, "Performance of monolayer graphene nanomechanical resonators with electrical readout." Nat. Nanotechnol. **4**, 861–7 (2009).

[18]X. Song, M. Oksanen, M. a. Sillanpää, H. G. Craighead, J. M. Parpia, and P. J. Hakonen, "Stamp transferred suspended graphene mechanical resonators for radio frequency electrical readout." Nano Lett. **12**, 198–202 (2012).

[19]D. M. KARABACAK, *resonance operation of nanoelectromechanical systels in fluidic environment*, Ph.D. thesis, BOSTON UNIVERSITY (2008).

[20]R. Lifshitz and M. L. Roukes, "Thermoelastic Damping in Micro- and Nano-Mechanical Systems," Phys. Rev. B **61**, 10 (1999), arXiv:9909271 [cond-mat].

[21]V. Gouttenoire, T. Barois, S. Perisanu, J.-L. Leclercq, S. T. Purcell, P. Vincent, and A. Ayari, "Digital and FM demodulation of a doubly clamped single-walled carbon-nanotube oscillator: towards a nanotube cell phone." Small **6**, 1060–5 (2010).

[22]A. M. Van Der Zande, R. a. Barton, J. S. Alden, C. S. Ruiz-Vargas, W. S. Whitney, P. H. Q. Pham, J. Park, J. M. Parpia, H. G. Craighead, and P. L. McEuen, "Large-Scale Arrays of Single-Layer Graphene Resonators." Nano Lett. , 4869–4873 (2010).

[23]A. K. Huttle, G. A. Steele, B. Witkamp, M. Poot, L. P. Kouwenhoven, and H. S. J. Van Der Zant, "Carbon nanotubes as ultrahigh quality factor mechanical resonator," Nano Lett. **9**, 2547–2552 (2009).

[24]M. Takamura, H. Okamoto, K. Furukawa, H. Yamaguchi, and H. Hibino, "Energy dissipation in edged and edgeless graphene mechanical resonators," J. Appl. Phys. **116**, 064304 (2014).

[25]G. K. White and J. G. Collins, "Thermal expansion of copper, silver, and gold at low temperatures," J. Low Temp. Phys. **7**, 43–75 (1972).

[26]F. C. Nix and D. MacNair, "Thermal expansion of pure metals, copper, gold, Aluminium, nickel and iron.pdf," Phys. Rev. Rev **60**, 597–605 (1941).

[27]K. G. Lyon, G. L. Salinger, C. a. Swenson, and G. K. White, "Linear thermal expansion measurements on silicon from 6 to 340 K," J. Appl. Phys. **48**, 865 (1977).

[28]N. Mounet and N. Marzari, "First-principles determination of the structural, vibrational and thermodynamic properties of diamond, graphite, and derivatives," Phys. Rev. B **71**, 1–14 (2005).

[29]D. Yoon, Y.-W. Son, and H. Cheong, "Negative thermal expansion coefficient of graphene measured by raman spectroscopy," Nano Lett. (2011).

[30]R. A. Suleimanov and N. A. Abdullaev, "The nature of negative linear expansion of graphite crystals," Carbon N. Y. **31**, 1011–1013 (1993).

[31]Z. Han, A. Kimouche, D. Kalita, A. Allain, H. Arjmandi-tash, A. Reserbat-Plantey, L. L. Marty, S. S. Pairis, V. V. Reita, N. Bendiab, J. Coraux, and V. Bouchiat, "Homogeneous Optical and Electronic Properties of Graphene Due to the Suppression of Multilayer Patches During CVD on Copper Foils," Adv. Funct. Mater. **24**, 964–970 (2014).

[32]R. J. T. Nicholl, H. J. Conley, N. V. Lavrik, I. Vlassiouk, Y. S. Puzyrev, P. S. T. Sreenivas, Vijayashree Parsi, and K. I. Bolotin, "The effect of intrinsic crumpling on the mechanics of free-standing graphene," Nature Communications (2015).

[33]G. Li, a. Luican, J. M. B. L. D. Santos, a. H. C. Neto, a. Reina, J. Kong, and E. Y. Andrei, "Observation of Van Hove singularities in twisted graphene layers," Nat. Phys. **6**, 21 (2009), arXiv:0912.2102.

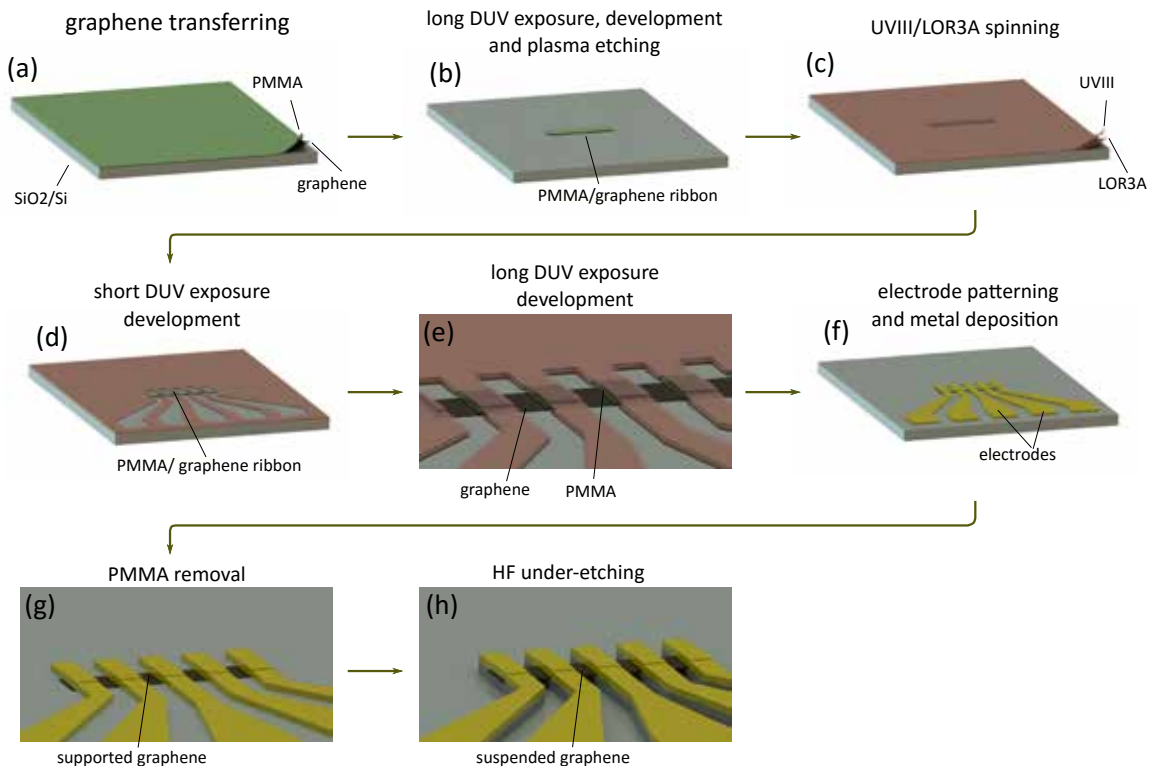

FIG. 4: Process flow of the *ribbon-blanketed* fabrication of the electrically connected CVD graphene based nano-mechanical resonators

a) PMMA supported CVD graphene is transferred onto a SiO_2/Si wafer.

b) Photolithography step and oxygen plasma etching pattern the PMMA/graphene into arrays of ribbons (only one is shown here).

c) The surface of the sample is spin-coated by LOR 3A and UVIII layers.

d) Photolithography followed by the development with resist is used to pattern the UVIII/LOR 3A layers with the design of the electrodes. Areas of the PMMA covered graphene ribbons are disclosed through the just-opened patterns and are ready for further DUV exposure.

e) Using the UVIII/LOR 3A mask, long photolithography exposes the uncovered areas of the PMMA. The exposed PMMA is developed with MIBK, disclosing the graphene ribbon(s) underneath.

f) Electrode materials (Cr, 5 nm and Au, 70 nm) are deposited. Lift-off is done with micro-developer to remove the unnecessary metal and UVIII/LOR 3A layers.

g) Blanketing PMMA is removed by acetone.

h) Uncovered graphene areas are under-etched with buffered HF solution and dried with a critical point dryer. Suspended and electrically connected graphene membranes are achieved.

Supplementary Information

Large scale integration of CVD-graphene based NEMS with narrow distribution of resonance parameters

Hadi Arjmandi-Tash,[1, a)] Adrien Allain,[1, b)] Zheng (Vitto) Han,[1, c)] and Vincent Bouchiat[1]

University of Grenoble Alpes, CNRS, Institut Néel, F-38000 Grenoble, France

[a)]h.arjmandi.tash@lic.leidenuniv.nl; Present address: Leiden Institute of Chemistry,Faculty of Science, Leiden University, Leiden, Netherlands

[b)]Present address: Laboratory of Nanoscale Electronics and Structures, École Polytechnique Fédérale de Lausanne, Station 17, CH-1015, Lausanne,Switzerland

[c)]Present address: Institute of Metal Research Chinese Academy of Sciences, Shenyang, Liaoning, 110016, China

I. MECHANICAL RESONANCES OF GRAPHENE RIBBONS

The fundamental resonance frequency of a flexural mode for a doubly clamped ribbon in the absence of built-in stress is given by [1–3]:

$$f_0(\Gamma = 0) = 1.03\sqrt{\left(\frac{E}{\rho}\right)\left(\frac{t^2}{L^4}\right)}. \tag{1}$$

In this equation, E, ρ, t and L respectively represent the Young's modulus, the mass density, the thickness and the length of the membrane. The above formula applied to our sample geometry predicts a resonance frequency of $\approx 3.9\,\mathrm{MHz}$ for our samples ($L = 1.3\,\mu m$), which clearly underestimate the experimental values presented in table 1, and point towards the presence of a finite residual stress within the membranes. Indeed fabrication process such as electrode deposition may stretch the membrane, inducing some tension which is referred to as the built-in tension (Γ_0). In the presence of stress, the frequency of the fundamental flexural mode becomes:

$$f_0(\Gamma_0, V_g) = \sqrt{\frac{\Gamma_0}{4m_{eff}L}} \tag{2}$$

In presence of a DC voltage , a mode softening (negative dispersion) upon is reproducibly seen. Similar negative dispersion behaviors have been reported earlier in graphene membranes [4,5] and nanowires [6–8] and are attributed to the mode softening as a result of the capacitive contribution to the energy of the resonator. For such systems, f_0 is modeled as:

$$f_0(\Gamma_0, V_g) = \overbrace{\sqrt{\frac{\Gamma_0}{4m_{eff}L}}}^{f_{max}} - \overbrace{\frac{C"}{8\pi^2}\sqrt{\frac{L}{m_{eff}\Gamma_0}}}^{\sigma} V_g^2. \tag{3}$$

Here, the term $C" = \partial^2 C/\partial z^2$ represents the second derivative of the capacitance between the membrane and the back gate (C) with respect to the small modulation of the membrane (z). m_{eff} approximates the sum of the mass of the membrane and the mass of the residual material on the membrane; m_{eff} is used to extract the relative density ($= \rho_{eff}/\rho_0$) where $\rho_0 = 7.6 \times 10^{-19} kg/\mu m^2$ is the mass density of bare monolayer graphene.

II. FITS OF THE EXPERIMENTAL DISPERSION CURVES

Experimental curves plotting the variation of resonance frequency of the graphene NEMS as a function of the backgate voltage can be fitted using previous equation (3), as seen in the figure below. For that particular case, one finds f_{max}=13.16 MHz and σ=-0.004 MHz, which leads to $m_{eff} = 2.3 \times 10^{-18}$kg , $C" = \partial^2 C/\partial z^2 = 1.6 \times 10^{-5} F/m^2, \Gamma_0 = 2.3 \times 10^{-9} N$

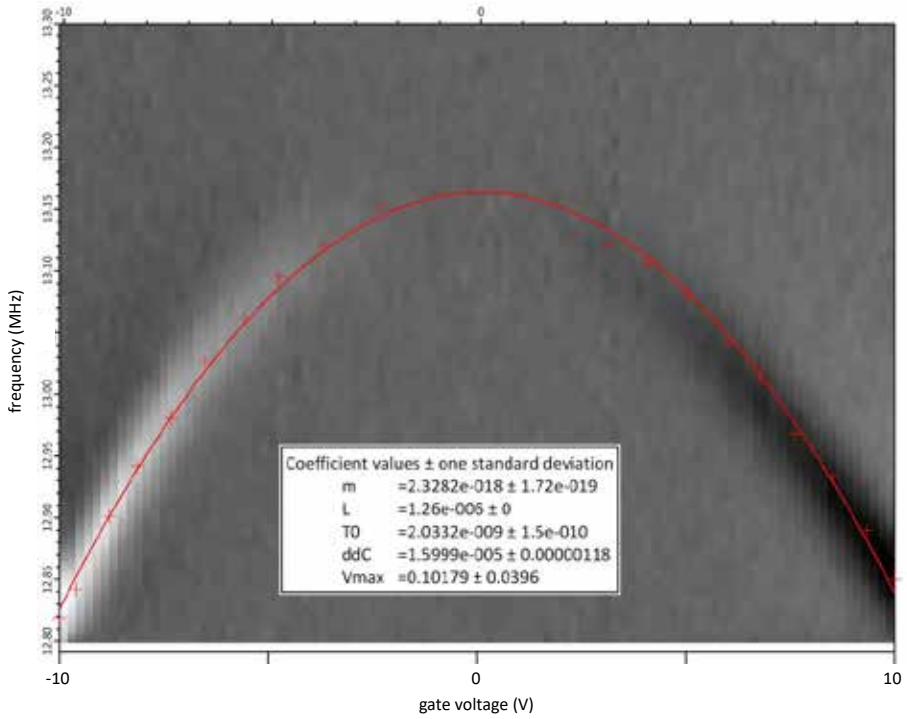

FIG. 1: Parameters extractions using fits of the dispersion curves. The full list of parameters extracted for those fits is shown in Table 1 of main article.

III. BENCHMARKING OF THE GRAPHENE NEMS WITH PREVIOUS RESULTS

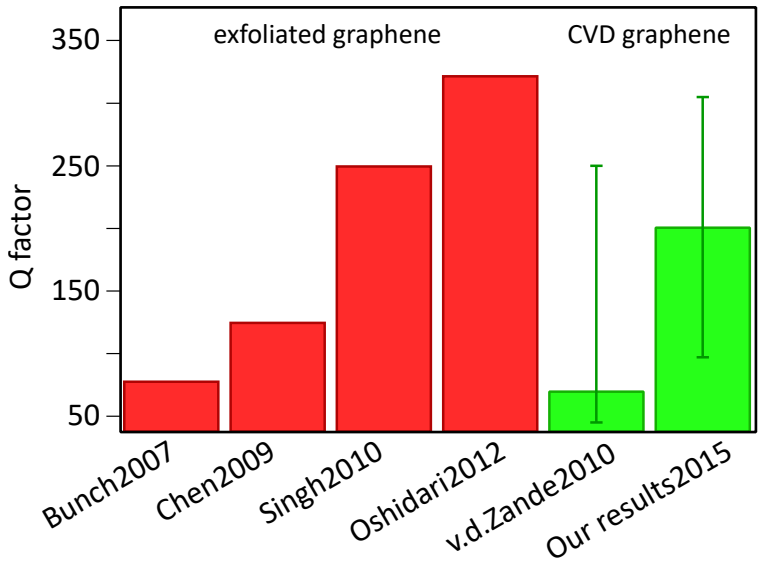

FIG. 2: Comparison of the quality factor of our samples (10 samples, $1\,\mu m \leq$ length $\leq 2.5\,\mu m$, $1\,\mu m \leq$ width $\leq 3.5\,\mu m$, $V_g = 10\,V$) with early reports of exfoliated (Bunch2007 [9], Chen2009 [1], Singh2010 [4], Oshidari2012 [10]) and CVD (v.d.Zande2010 [11]) graphene membranes: Only the *room-temperature* reports of *doubly-clamped* nano-mechanical resonators with *monolayer* graphene membranes are collected here.

IV. CALCULATION OF THE MASS SENSITIVITY

Minimum resolvable mass (δm) of a resonator with the effective mass and quality factor of m_{eff} and Q, is estimated as[12]:

$$\delta m = \frac{m_{eff}}{Q} \times 10^{\frac{-DR}{20}} \tag{4}$$

Here DR, expressed in decibels (dB), is the dynamic range of the resonator and corresponds the ratio of the highest achievable signal level (before the onset of a nonlinear behavior) over the lowest measurable signal level [6]. To estimate the DR, we recorded the response of the device both in forwards and backwards sweeps (shown only for some of the curves) while gradually increasing the driving potential (Figure 3). The scheme let us to probe the signal upto $V_{ds} = 350\,mV$: up to this potential, the device did not enter into

nonlinear regime as the response does not show any hysteresis (perfect overlap of forward and backward sweeps). The signal at the highest V_{ds} before entering the nonlinear divided by the rms noise gives a lower limit for the dynamic range as: $DR > 61.5\,dB$.

m_{eff} in Equation 4 is achievable by probing the gate dependence of the resonance frequency. As seen in Fig. S1, $m_{eff} = 2.3 \times 10^{-18}\,kg$ for this device.

Quality factor is the other parameter in Equation 4: We estimate it by fitting the signal with the model proposed by [13] for frequency modulation actuation and detection scheme:

$$I(\omega_c) = \frac{2\omega_c \left(\omega_c^2 - \omega_0^2 - \frac{\omega_0^2}{Q}\right)\left(\omega_c^2 - \omega_0^2 + \frac{\omega_0^2}{Q}\right)}{\left[\left(\omega_0^2 - \omega_c^2\right)^2 + \left(\frac{\omega_0 \omega_c}{Q}\right)^2\right]^2} \tag{5}$$

$I(\omega_c)$, ω_c and ω_0 are respectively the measured current at the drain electrode, carrier frequency and the natural oscillation frequency of the resonator. The dotted curve in the inset of Figure 3 shows the best fitting of the resonance peak with $V_ds = 20\,mV$ with this model, revealing the quality factor of 236.

Using the parameters achieved and by employing the Equation 4, we estimate the mass resolution of this device to be better than $8.2 \times 10^{-21}\,g$.

V. CALCULATION OF THE FORCE SENSING THRESHOLD

The minimum resolvable force (δF) of a resonator at temperature T is determined by the force spectral density as:

$$\delta F = \sqrt{\frac{4 k_b T m_{eff} \omega_0}{Q}} \tag{6}$$

where $k_b = 1.38 \times 10^{-23}\,m^2 kg/s^2 K$ is the Boltzmann constant. Using the parameters achieved in the former section, we estimated $\delta F = 44.8\,aN/\sqrt{Hz}$ for our device.

VI. FUNDAMENTAL LIMITATION OF THE QUALITY FACTOR DUE TO THE THERMOELASTIC DAMPING

Thermoelastic damping sets a fundamental limitation for the quality factor of a resonator [14]. Via this mechanism, the nonlinear interaction of an elastic resonator (oscillating

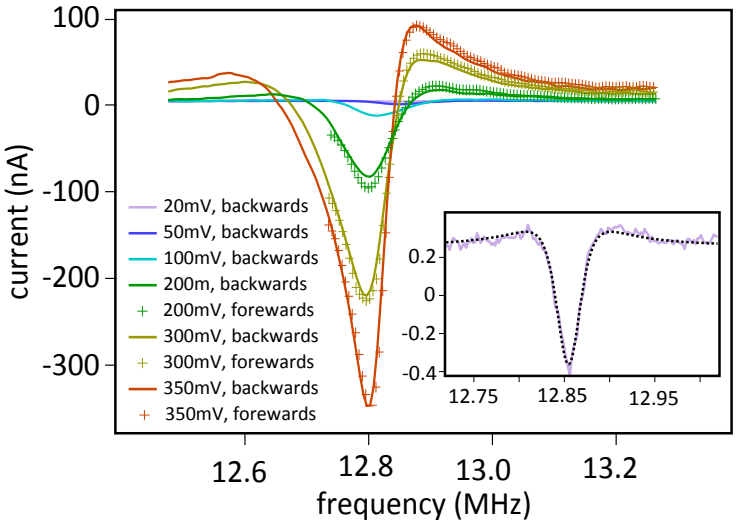

FIG. 3: Linearity analysis to estimate of the dynamic range

Main panel): Resonance peak of a device as function of the driving potential: both forward and backward sweeps are plotted for the three highest drive voltages.

Inset): Resonance peak with the lowest drive potential ($20\,mV$): the dotted line is the best fit obtained using the equation of the resonance peak in frequency modulation scheme [13].

The experiments were performed at $V_g = -10V$. The device is the same as discussed as in Figure 3-a of the main text.

at its normal mode) with thermally excited elastic modes or phonons of the environment dissipates the energy. The mechanism sets an upper value for the Q factor given by [14]:

$$Q_{max}^{TE\,-1} = 0.494\,\frac{E\alpha^2 T}{\rho\, C_{p,m}} \tag{7}$$

We use the values in Table I and estimated $Q_{max}^{TE} = 308$ in graphene.

TABLE I: Parameters used to calculate Q_{max}^{TE} in Equation 7

parameter	value	reference
E: Young's modulus	1 TPa	[15]
α: thermal expansion coefficient	$-3.8 \times 10^{-6}\,K^{-1}$	main text
T: temperature	300 K	-
ρ: density	$2200\,kg\,m^{-3}$	[16]
$C_{p,m}$: heat capacity per unit mass at constant pressure	$\sim 300\,J\,kg^{-1}K^{-1}$	[17]

VII. CALCULATION OF THE COEFFICIENT OF THE THERMAL EXPANSION (CTE) OF CVD GRAPHENE

At least two theory papers have calculated the CTE for graphite and graphene [18,19] predicting negative CTE due to the out of plane vibrations of the lattice. Bao *et al* [20] first investigated the CTE of suspended graphene experimentally in the temperature range of 300 K to 400 K obtaining $\alpha_{300\,K} \approx -7 \times 10^{-6}\,K^{-1}$. Next, Chen *et al* [1] reported a constant $\alpha = -7.4 \times 10^{-6}\,K^{-1}$ in a small temperature range below room temperature (250 K to 295 K). The work was followed by Singh *et al* [4] in a wider temperature range (30 K to 300 K). All those experimental works performed using suspended and exfoliated graphene. Later, Yoon *et al* [21] also estimated the CTE of supported exfoliated graphene by examining strain-related Raman fingerprints of graphene [21]. Figure 3-c in the main text reprints and compares all the results reported at $T \leq 300\,K$.

Here we use the model presented by Singh *et al* [4] to study the CTE of CVD graphene. As the device cools down from room temperature, the suspended gold electrodes start to contract which tends to increase the tension in the membrane; however the contraction of the silicon wafer and expansion of the graphene (due to its negative CTE) lower the tension (inset Figure 4-a). Equation 8 explains the relation among the strained materials:

$$\epsilon_{mem}(T) = \epsilon_{gr}(T) + \epsilon_{w}(T) - \frac{w_e}{L}\epsilon_{e}(T). \tag{8}$$

Here, ϵ_{mem}, ϵ_{gr}, ϵ_{w} and ϵ_{e} denote the temperature dependent strain of the membrane (clamped graphene), the free (not clamped) graphene, the wafer and the electrodes, respectively. Note that the relation $\frac{d}{dT}\epsilon_{w,\,e,\,gr} = \alpha_{w,\,e\,gr}$ holds to describe the temperature induced strain and the corresponding CTE. w_e and L are geometrical parameters and represent the width of the electrodes and the length of the membrane. The data of α_w and α_e in the temperature range of our interest have been reported before (re-plotted in Figure 4-a). Additionally, $\epsilon_{mem}(T)$ can be estimated following the temperature-dependent resonance frequency ($f_0(T)$) of the membrane:

$$\epsilon_{mem}(T) = \frac{\Gamma(T) - \Gamma(T = 300\,K)}{wtE_{gr}} \tag{9}$$

where:

$$\Gamma(T) = 4L^2 f_0(T)^2 \rho t w \tag{10}$$

Here, E_{gr} [15] is the Young's modulus, t is the thickness, ρ is the mass density and w is the width of the monolayer graphene membrane. Using Equations 8 to 10 and assuming uniform expansions for all the materials, one can calculate α_{gr} as:

$$\alpha_{gr}(T) = -\frac{8L^2\rho}{E_{gr}}\omega_n \frac{d\omega_n}{dT} + \left(\alpha_w(T) - \frac{w_e}{L}\alpha_e(T)\right). \tag{11}$$

Several sources of uncertainties are considered in our estimation:

- By starting the cooling contamination and/or humidity in the measurement set-up deposited on the membrane which may account for a rapid jump in the resonance frequency. As the actual frequency of the sample in the absence of this deposited materials is unknown, we considered the green-shaded area in Figure 4-b as the uncertainty range in $f_0(T)$.

- Although E = 1 TPa is a generally accepted value for the Young's modulus of graphene[15], recent measurements have reported values of few times lower[22 23] which is considered as another source of uncertainty in our calculations.

- The model of Equation 11 assumes the Au electrodes, where they cover the graphene ribbon, are fully suspended. Depending on the etching duration, this assumption might/might not be correct. Also the effect of the supported parts of the electrodes (just besides the graphene ribbon) in constraining the free straining of the electrodes are overlooked. To consider all these effects, we allow up to 50% error in estimating the straining of the electrodes.

- Our measurements of the length of the membrane is based on the SEM images of the samples. We allowed upto 20% error in our estimation.

Considering all the uncertainties listed above, we estimated the CTE of CVD graphene as plotted in Figure 3-c in the main text.

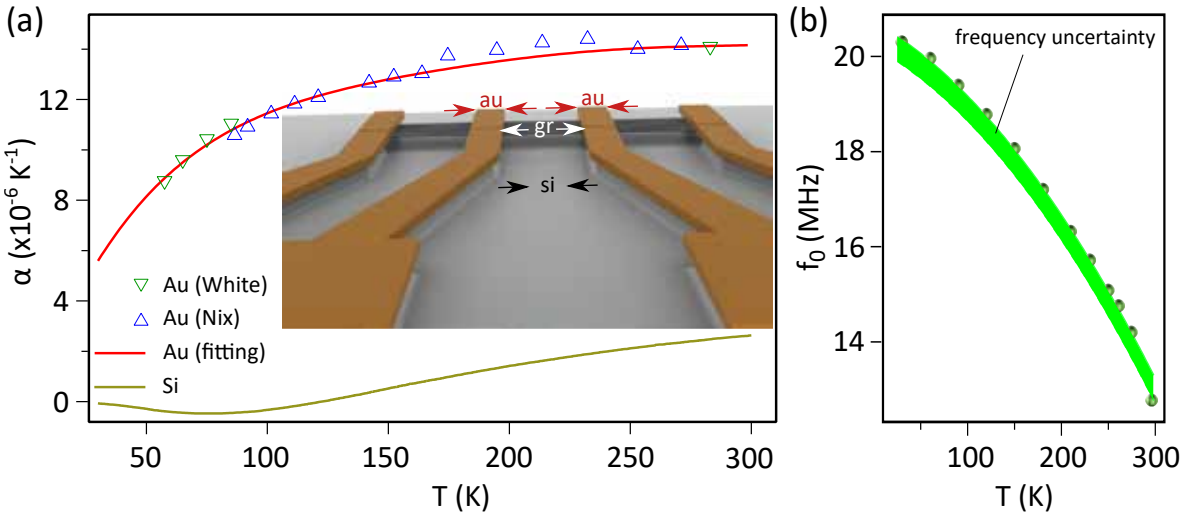

FIG. 4: Parameters involved in the calculation of the CTE of CVD graphene a) Temperature dependent CTE of gold and silicon: Au (White) and Au (Nix) refer to the data points reported for Au films, respectively by Ref.[24] and Ref.[25] and the red line is the best fitting (polynomial function) for those data points. The CTE for silicon are reprinted from Ref.[26]. The inset shows the expansion/contraction of different materials involved, upon cooling the system.

b) Experimentally measured temperature dependent frequency of a CVD graphene nanoresonator: A rapid jup between the first and second data points is observed. The continuous line is the best fitting (polynomial function) for the data points after the rapid jump. The uncertainty of the frequency is estimated by the green-shaded area.

REFERENCES

[1]C. Chen, S. Rosenblatt, K. I. Bolotin, W. Kalb, P. Kim, I. Kymissis, H. L. Stormer, T. F. Heinz, and J. Hone, "Performance of monolayer graphene nanomechanical resonators with electrical readout." Nat. Nanotechnol. **4**, 861–7 (2009).

[2]W. Weaver, Jr., S. P. Timoshenko, and D. H. Young, *Vibration Problems in Engineering* (1990).

[3]S. Shivaraman, R. a. Barton, X. Yu, J. Alden, L. Herman, M. S. V. Chandrashekhar, J. Park, P. L. McEuen, J. M. Parpia, H. G. Craighead, and M. G. Spencer, "Free-standing epitaxial graphene," Nano Lett. **9**, 3100–3105 (2009).

[4]V. Singh, S. Sengupta, H. S. Solanki, R. Dhall, A. Allain, S. Dhara, P. Pant, and

M. M. Deshmukh, "Probing thermal expansion of graphene and modal dispersion at low-temperature using graphene nanoelectromechanical systems resonators." Nanotechnology **21**, 165204 (2010).

[5]X. Song, M. Oksanen, M. a. Sillanpää, H. G. Craighead, J. M. Parpia, and P. J. Hakonen, "Stamp transferred suspended graphene mechanical resonators for radio frequency electrical readout." Nano Lett. **12**, 198–202 (2012).

[6]I. Kozinsky, H. W. C. Postma, I. Bargatin, and M. L. Roukes, "Tuning nonlinearity, dynamic range, and frequency of nanomechanical resonators," Appl. Phys. Lett. **88**, 253101 (2006).

[7]H. S. Solanki, S. Sengupta, S. Dhara, V. Singh, S. Patil, R. Dhall, J. Parpia, A. Bhattacharya, and M. M. Deshmukh, "Tuning mechanical modes and influence of charge screening in nanowire resonators," Phys. Rev. B **81**, 115459 (2010).

[8]A. Eichler, J. Moser, J. Chaste, M. Zdrojek, I. Wilson-Rae, A. Bachtold, and I. W. Rae, "Nonlinear damping in mechanical resonators made from carbon nanotubes and graphene SOI," Nat. Nanotechnol. **6**, 339–42 (2011).

[9]J. S. Bunch, A. M. van der Zande, S. S. Verbridge, I. W. Frank, D. M. Tanenbaum, J. M. Parpia, H. G. Craighead, and P. L. McEuen, "Electromechanical Resonators from Graphene Sheets," Science (80-.). **315**, 490–493 (2007).

[10]Y. Oshidari, T. Hatakeyama, R. Kometani, S. Warisawa, and S. Ishihara, "High Quality Factor Graphene Resonator Fabrication Using Resist Shrinkage-Induced Strain," Appl. Phys. Express **5**, 117201 (2012).

[11]A. M. Van Der Zande, R. a. Barton, J. S. Alden, C. S. Ruiz-Vargas, W. S. Whitney, P. H. Q. Pham, J. Park, J. M. Parpia, H. G. Craighead, and P. L. McEuen, "Large-Scale Arrays of Single-Layer Graphene Resonators." Nano Lett. , 4869–4873 (2010).

[12]K. L. Ekinci and M. L. Roukes, "Nanoelectromechanical systems," Rev. Sci. Instrum. **76**, 061101 (2005).

[13]V. Gouttenoire, T. Barois, S. Perisanu, J.-L. Leclercq, S. T. Purcell, P. Vincent, and A. Ayari, "Digital and FM demodulation of a doubly clamped single-walled carbon-nanotube oscillator: towards a nanotube cell phone." Small **6**, 1060–5 (2010).

[14]R. Lifshitz and M. L. Roukes, "Thermoelastic Damping in Micro- and Nano-Mechanical Systems," Phys. Rev. B **61**, 10 (1999), arXiv:9909271 [cond-mat].

[15]C. Lee, X. Wei, J. W. Kysar, and J. Hone, "Measurement of the elastic properties and

intrinsic strength of monolayer graphene." Science **321**, 385–8 (2008).

[16]D. Garcia-Sanchez, a. M. van der Zande, a. S. Paulo, B. Lassagne, P. L. McEuen, and A. Bachtold, "Imaging mechanical vibrations in suspended graphene sheets." Nano Lett. **8**, 1399–403 (2008).

[17]E. Pop, V. Varshney, and A. K. Roy, "Thermal properties of graphene: Fundamentals and applications," MRS Bull. **37**, 1273–1281 (2012).

[18]R. A. Suleimanov and N. A. Abdullaev, "The nature of negative linear expansion of graphite crystals," Carbon N. Y. **31**, 1011–1013 (1993).

[19]N. Mounet and N. Marzari, "First-principles determination of the structural, vibrational and thermodynamic properties of diamond, graphite, and derivatives," Phys. Rev. B **71**, 1–14 (2005).

[20]W. Bao, F. Miao, Z. Chen, H. Zhang, W. Jang, C. Dames, and C. N. Lau, "Controlled ripple texturing of suspended graphene and ultrathin graphite membranes." Nat. Nanotechnol. **4**, 562–6 (2009).

[21]D. Yoon, Y.-W. Son, and H. Cheong, "Negative thermal expansion coefficient of graphene measured by raman spectroscopy," Nano Lett. (2011).

[22]R. J. T. Nicholl, H. J. Conley, N. V. Lavrik, I. Vlassiouk, Y. S. Puzyrev, P. S. T. Sreenivas, Vijayashree Parsi, and K. I. Bolotin, "The effect of intrinsic crumpling on the mechanics of free-standing graphene," Nature Communications (2015).

[23]C. S. Ruiz-Vargas, H. L. Zhuang, A. M. Huang, Pinshane Y annd van der Zande, S. Garg, P. L. McEuen, D. A. Muller, R. G. Hennig, and J. Park, "Softened elastic response and unzipping in chemical vapor deposition graphene membranes," Nano Lett. (2011).

[24]G. K. White and J. G. Collins, "Thermal expansion of copper, silver, and gold at low temperatures," J. Low Temp. Phys. **7**, 43–75 (1972).

[25]F. C. Nix and D. MacNair, "Thermal expansion of pure metals, copper, gold, Aluminium, nickel and iron.pdf," Phys. Rev. Rev **60**, 597–605 (1941).

[26]K. G. Lyon, G. L. Salinger, C. a. Swenson, and G. K. White, "Linear thermal expansion measurements on silicon from 6 to 340 K," J. Appl. Phys. **48**, 865 (1977).